Supporting Information for

A bimodal time-gated luminescence-magnetic resonance imaging nanoprobe based on europium(III) complex-BSA anchored MnO_2 nanosheets for highly selective detection of H_2O_2

Bo Song,*[a] Ziyao Wang,[a] Huinan Yan,[a] Xinyue Zhang,[a] Qi Liu,[a] Jiawen Luo,*[b] and Jingli Yuan [c]

[a] State Key Laboratory of Fine Chemicals, School of Chemical Engineering, Dalian University of Technology, Dalian 116024, China.

[b] Department of Radiology, The Second Affiliated Hospital of Dalian Medical University, Dalian, Liaoning, China

[c] College of Life Science, Dalian Minzu University, 18 Liaohe West Road, Jinzhou New District, Dalian 116600, China

E-mail: bo.song@dlut.edu.cn, kaoyan2006succeed@163.com

Table of Contents

1. Experimental section

Materials and physical measurements

The visible-light-excitable β-diketone-Eu^{3+} complex were prepared according to the previously reported methods.[1-3] manganese chloride tetrahydrate ($MnCl_2 \cdot 4H_2O$), hydrogen peroxide (H_2O_2, 30 wt%), L-glutathione (GSH), N-ethylmaleimide (NEM), N-acetyl-L-cysteine (NAC) and 3-(4,5-dimethyl-2-thiazoyl)-2,5-diphenyltetrazolium bromide (MTT) were purchased from Sigma-Aldrich. Cultured HeLa, BALB/c mice were provided by Dalian Medical University. Unless otherwise stated, all chemical materials were purchased from commercial sources and used without further purification.

The morphology of BSA@MnO_2 nanosheets was characterized with a JEOL JEM-2000EX transmission electron microscope (TEM). Zeta potential and dynamic light scattering (DLS) were measured by using Zetasizer Nano ZS90 UK. FT-IR were measured by using Thermo Fisher iS50 USA.The AFM images of BSA@MnO_2 nanosheets were recorded on a Bruker Nanowizard 4XP atomic force microscope. The contents of Mn were measured on a PerkinElmer Optima 2000DV inductively coupled plasma-optical emission spectrometer (ICP-OES). TGL spectra were measured on a Perkin-Elmer LS 50B luminescence spectrometer with the settings of delay time, 0.2 ms; gate time, 0.4 ms; cycle time, 20 ms; excitation slit, 8 nm; and emission slit, 8 nm. Absorption spectra were measured on a UV-1800 UV-Vis spectrophotometer (Shimadzu Instruments Suzhou Co., Ltd.). Luminescence lifetimes were measured on an Edinburgh FS5 spectrometer. All bright-field, steady-state and TGL imaging measurements were conducted on a laboratory-use luminescence microscope. The measurements of transverse and longitudinal relaxation times were performed on a 0.5 T NM12 MR analyzer (Suzhou Niumag Analytical Instrument Corporation). All the MRI measurements were carried out on an NMI20-030H-I MR imager (Suzhou Niumag Analytical Instrument Corporation).

Preparation of the nanoprobe and its application to bimodal TGL-MR detections of GSH and H_2O_2 in buffer

Cyclic voltammetric (CV) analyses were carried out on an autolab electrochemical system

(CHI600D, Shanghai) coupled with a three-electrode cell. The working electrode was a glassy carbon electrode, the auxiliary electrode was a platinum wire and all the potentials reported in this study have been measured against Ag/AgCl as a reference electrode. All the CV measurements were carried out at room temperature in a solution of 20 mL HEPES buffer (10 mM, pH = 7.4). The scanned area was in the potential range of -1.5 V to 1.4 V and the scan rate was 0.1 V/s. The $MnCl_2$ solution was chosen as the standard Mn^{2+} solution (120 μM). In order to verify H_2O_2-triggered the reduction of BSA@MnO_2 nanosheets to Mn^{2+} , the BSA@MnO_2 nanosheets and H_2O_2-BSA@MnO_2 nanosheets (120 μM BSA@MnO_2 nanosheets were incubated with 120 μM H_2O_2 for 8 min at room temperature) were subjected to CV measurements.

For TGL detections of H_2O_2 in buffer, the nanoprobe [$Eu(BTD)_3$(DPBT)]-BSA@MnO_2 was prepared by incubating 2.0 μM [$Eu(BTD)_3$(DPBT)] with 180 μM BSA@MnO_2 nanosheets for 2 min at RT in 0.01 M HEPES buffer (pH 7.4, containing 0.05% Triton X-100). The obtained nanoprobe solution was mixed with different concentrations of H_2O_2 for 10 min, and then the mixtures were subjected to TGL measurements.

For MR detections of H_2O_2 in buffer, the above as-prepared nanoprobe was mixed with various concentrations of H_2O_2 for 10 min. Then, the longitudinal and transverse relaxation times and MR images of the mixtures were measured on the MR analyzer and imager, respectively. For assessing the amount of free [$Eu(BTD)_3$(DPBT)] in the nanoprobe solution, the stock solution of [$Eu(BTD)_3$(DPBT)]-BSA@MnO_2 was separated by centrifugation using an Amicon Ultra centrifugal filter unit (pore size 10 kDa MWCO). The content of free [$Eu(BTD)_3$(DPBT)] in filtrate was evaluated by the TGL assay.

Response specificity investigation of the nanoprobe

To assess the response specificity of the nanoprobe to H_2O_2, the above as-prepared nanoprobe [$Eu(BTD)_3$(DPBT)]-BSA@MnO_2 was incubated with H_2O_2 (0.5 mM) and other interferents (1.0 mM) for 10 min, respectively. Then the TGL intensities and the transverse relaxation times of the mixtures were recorded.

Cytotoxicity and biocompatibility investigations of the nanoprobe

The cytotoxicity of the above as-prepared nanoprobe [$Eu(BTD)_3$(DPBT)]-BSA@MnO_2 to

HeLa cells was determined by MTT assay.[4] HeLa cells cultured in Dulbecco's modified Eagle medium (DMEM) were washed with isotonic saline (ISS, 140 mM NaCl, 10 mM glucose, 3.5 mM KCl) before use, and then incubated with different concentrations of $Eu(BTD)_3(DPBT)$-$BSA@MnO_2$ (0, 100, 200, 300, 400, 500, 600, 700, and 800 μM in Mn concentration) at 37 °C in a 5% CO_2 /95% air incubator for 24 h. After that, the cells were washed with ISS and incubated with 5 mg mL^{-1} MTT in an incubator for 4 h. After supernatants were removed, the cells was dissolved in 100 μL DMSO and the absorbance at 490 nm was measured.

To further examine the biocompatibility of the nanoprobe $[Eu(BTD)_3(DPBT)]$-$BSA@MnO_2$, three BALB/c mice (females, ~20 g body weight) were given $[Eu(BTD)_3(DPBT)]$-$BSA@MnO_2$ (250 μL, 11.5 μM $[Eu(BTD)_3(DPBT)]$ mixed with 1.0 mM $BSA@MnO_2$ nanosheets in physiological saline solution) by intravenous injection. After 24 h, the mice were sacrificed by dislocating cervical vertebra and the main organs (heart, liver, spleen, lung, and kidney) were surgically dissected. The collected organs were fixed with 4% formaldehyde in PBS and embedded in paraffin. Then the standard hematoxylin and eosin (H&E) staining was carried out for histological analysis.

TGL imaging of H_2O_2 in living cells

HeLa (human cervical adenocarcinoma cell line) were cultured in a glass bottom culture dishes in DMEM with 10% fetal bovine serum, 1% penicillin and 1% streptomycin at 37 °C in a 5% CO_2/95% air incubator. For staining cells, the cultured cells were washed three times with ISS, and then incubated with the nanoprobe $[Eu(BTD)_3(DPBT)]$-$BSA@MnO_2$ (8.0 μM $[Eu(BTD)_3(DPBT)]$ mixed with 720 μM $BSA@MnO_2$ nanosheets) in 500 μl culture medium for 4 h. After thoroughly washing with ISS, the cells were subjected to the TGLI on the microscope with the conditions of gate time, 1.0 ms; delay time, 10 μs; lamp pulse width, 60 μs; and exposure time, 500 ms. For the control group, HeLa cells were pretreated with 50 μM NAC for 0.5 h, 50 μM NEM for 0.5 h, 1 mM GSH for 0.5 h, 100 μM H_2O_2 for 0.5 h or 500 μM APAP for 0.5 h, respectively, and then incubated with the nanoprobe for 4 h prior to being used for TGLI.

Bimodal TGLI-MRI of H_2O_2 in tumor-bearing mice

To evaluate the performance of the nanoprobe [Eu(BTD)$_3$(DPBT)]-BSA@MnO_2 for TGLI-MRI of H_2O_2 *in vivo*, the tumor xenograft models were established by implanting H22 cells (mouse hepatoma cell line) in the subcutaneous tissue of BALB/c nude mice (female) with a bodyweight of ~20 g. After the tumor size reached to 1.5~2 cm in diameter, nine tumor-bearing BALB/c nude mice were randomly divided into three equal groups. For the experimental group, three mice were intravenously administered with 150 μL physiological saline solution containing the nanoprobe (11.5 μM [Eu(BTD)$_3$(DPBT)] mixed with 1.0 mM BSA@MnO_2 nanosheets). After that, the T_2-weighted MR images of the mice were taken at different time points (0, 0.5, 1, 2, 4 and 24 hour) following the injection. The MRI T_2 signal intensity analyses of the region of interest (ROI) were conducted using the Horos v3.3.1 software for Macintosh. To qualify the signal enhancement, the signal-to-noise ratio (SNR) was determined using the formula: $SNR = SI_{tumor}/SD_{noise}$, where SI and SD represent signal intensity and s.d, respectively. In NAC-treated group, the three tumor-bearing BALB/c nude mice peritumorally injected with 150 μL physiological saline solution containing 2.0 mM NAC. After 0.5 h, a physiological saline solution containing the nanoprobe was further intravenously injected into the mice. Then the tumors were successively monitored by T_2-weighted MRI. In addition, the above described mice were killed at 1 h post-injection of the nanoprobe, and the tumors were excised and stored at -20 ^oC for 24 h. The frozen tumor tissues were cryosectioned via microtome at -20 ^oC into slices of 30 μm thicknesses for the TGLI measurements on the microscope.

All of above animal studies were conducted in agreement with the guidelines of the Institutional Animal Care (No. 211003700000860) approved by the Animal Ethical and Welfare Committee (AEWC) of Dalian Medical University.

Statistical analysis

All the experiments were performed three times and the values were presented as the mean ± SD. Statistical comparison between the two groups was determined by Student's test. All statistical analyses were conducted with Excel (*$P < 0.05$, **$P < 0.01$, ***$P < 0.001$). A value of $P < 0.05$ was considered statistically significant.

2. Characterization of BSA@MnO_2 nanosheets

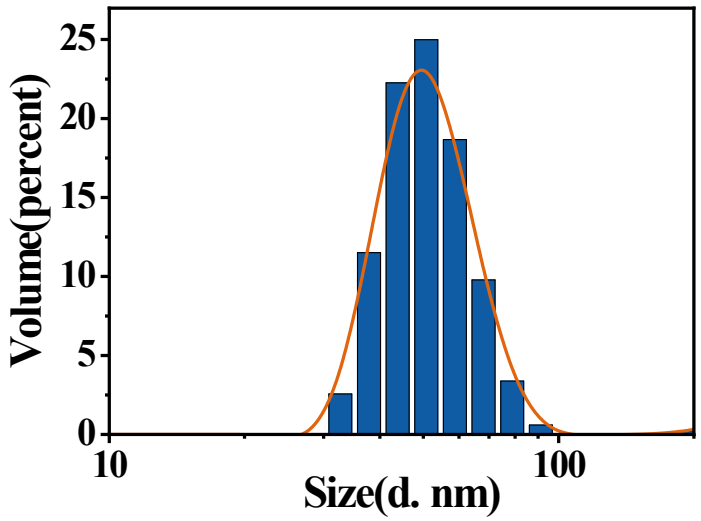

Fig. S1 Hydrated particle size distributions of BSA@MnO_2 nanosheets in 0.01M HEPES buffer (pH = 7.4, containing 0.05% Triton X-100) determined by DLS.

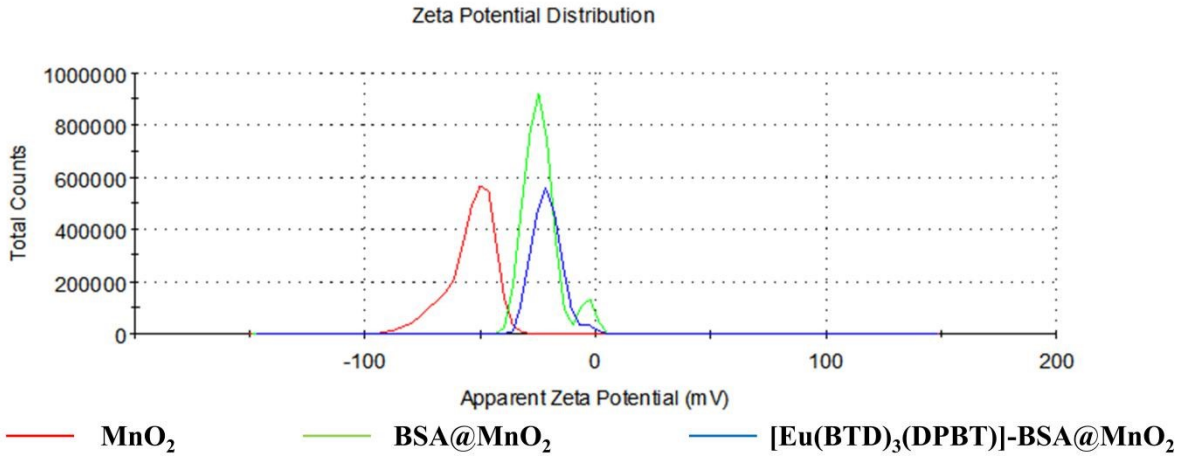

Fig. S2 Zeta potential distributions of MnO_2 nanosheets, BSA@MnO_2 nanosheets and [$Eu(BTD)_3(DPBT)$]-BSA@MnO_2 nanoprobe in 0.01M HEPES buffer (pH = 7.4, containing 0.05% Triton X-100).

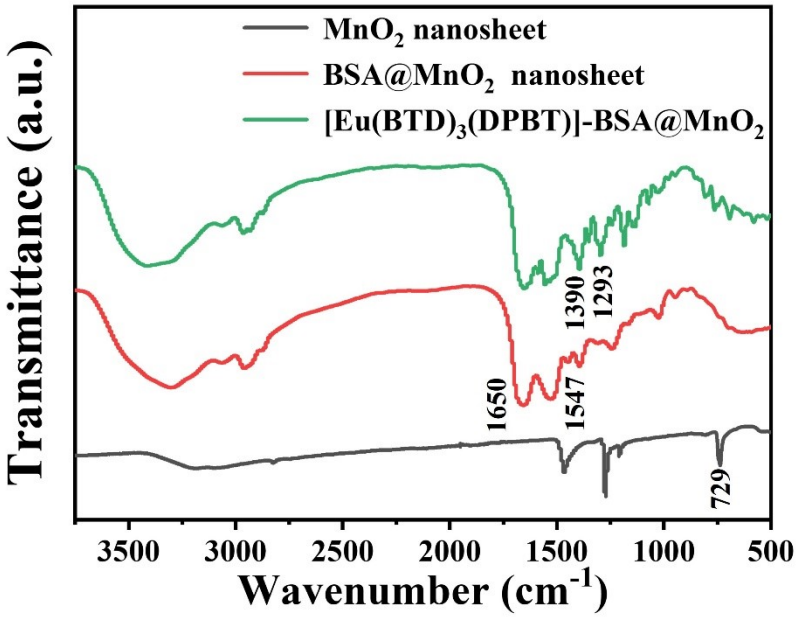

Fig. S3 FT-IR spectra of MnO_2 nanosheets, BSA@MnO_2 nanosheets, and [Eu(BTD)$_3$(DPBT)]-BSA@MnO_2 nanoprobe.

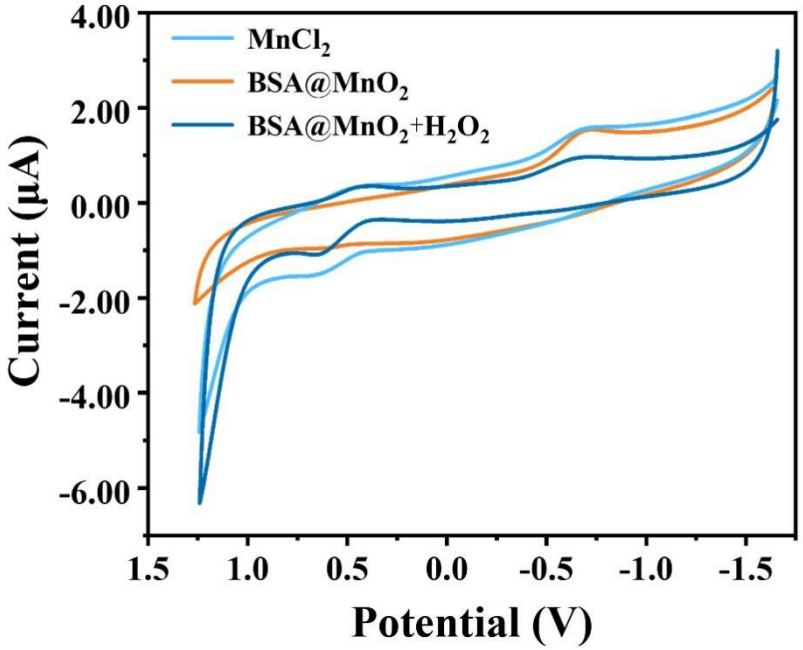

Fig. S4 CV profiles of Mn^{2+}, BSA@MnO_2 nanosheets in the absence and presence of H_2O_2

3. Luminescence properties of [Eu(BTD)$_3$(DPBT)]

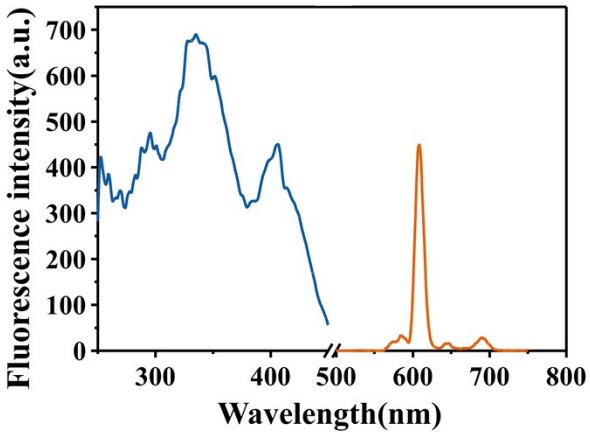

Fig. S5 Time-gated excitation (λ_{em} = 609 nm) and emission spectra (λ_{ex} = 406 nm) of [Eu(BTD)$_3$(DPBT)] (1.0 μM) in 0.01 M HEPES buffer (pH = 7.4, containing 0.05% Triton X-100).

Table S1 Luminescence properties of [Eu(BTD)$_3$(DPBT)]

	$\lambda_{ex,max}$ (nm)	$\lambda_{em,max}$ (nm)	ε ($cm^{-1}M^{-1}$)	τ (μs)	φ
[Eu(BTD)$_3$(DPBT)]	406	609	6.59×10^4	461	20.5%

4. Bimodal TGL-MR responses of the nanoprobe [Eu(BTD)$_3$(DPBT)]-BSA@MnO$_2$ to H$_2$O$_2$

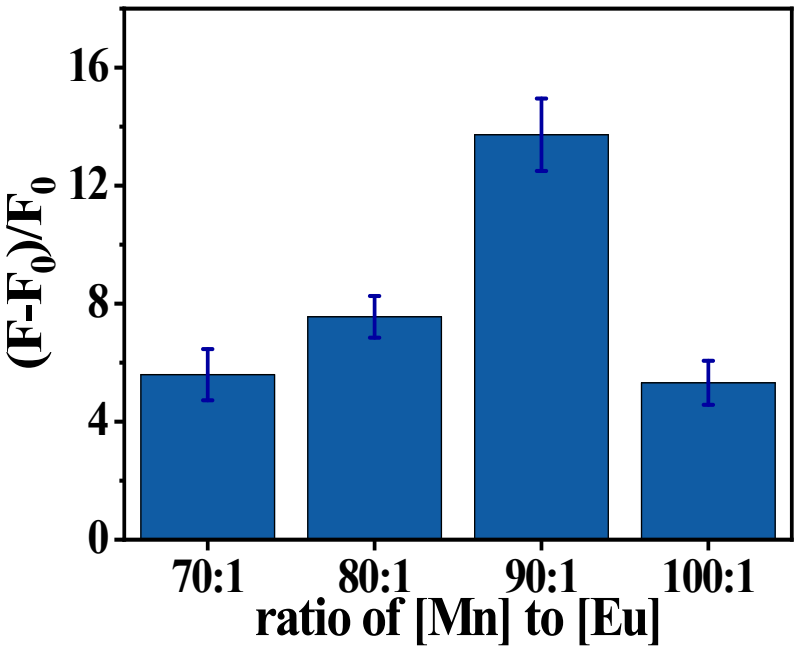

Fig. S6 TGL responses of the mixed solutions of 2.0 μM [Eu(BTD)$_3$(DPBT)] with different concentrations of BSA@MnO$_2$ nanosheets towards 50 μM H$_2$O$_2$ (F$_0$: TGL intensity of [Eu(BTD)$_3$(DPBT)]-BSA@MnO$_2$ in the absence of H$_2$O$_2$; F: TGL intensity of [Eu(BTD)$_3$(DPBT)]-BSA@MnO$_2$ reacted with H$_2$O$_2$.

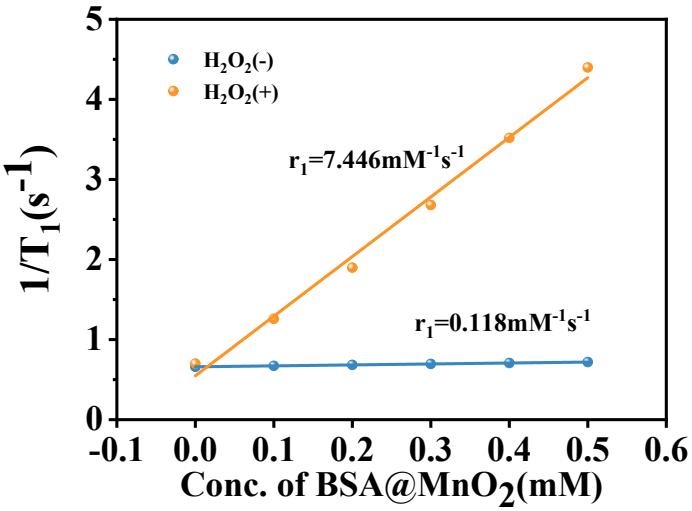

Fig. S7 Longitudinal relaxivity of the nanoprobe [Eu(BTD)$_3$(DPBT)]-BSA@MnO$_2$ in the absence and presence of H$_2$O$_2$.

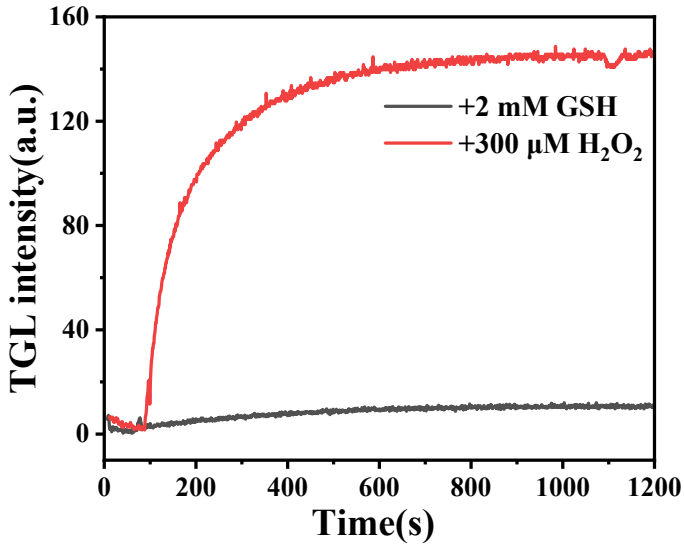

Fig. S8 Time-dependent changes of the TGL of [Eu(BTD)$_3$(DPBT)]-BSA@MnO$_2$ upon additions of H_2O_2 (300 μM) and GSH (2 mM).

5. Cytotoxicity and biocompatibility of the nanoprobe [Eu(BTD)$_3$(DPBT)] -BSA@MnO$_2$

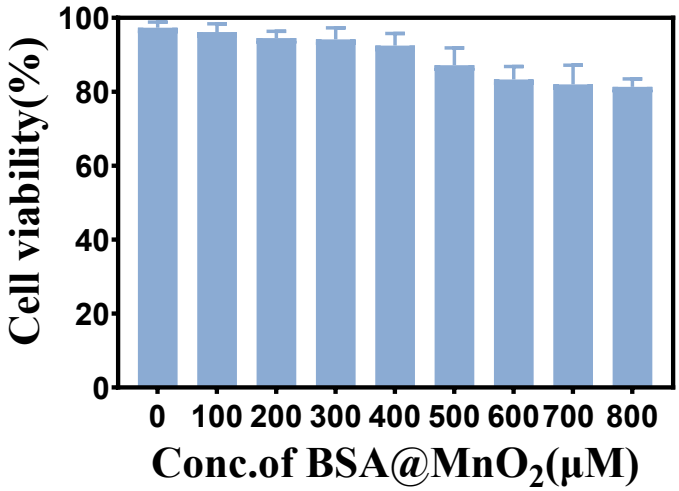

Fig. S9 Viabilities of HeLa cells incubated with different concentrations of the nanoprobe [Eu(BTD)$_3$(DPBT)]-BSA@MnO$_2$ for 24 h.

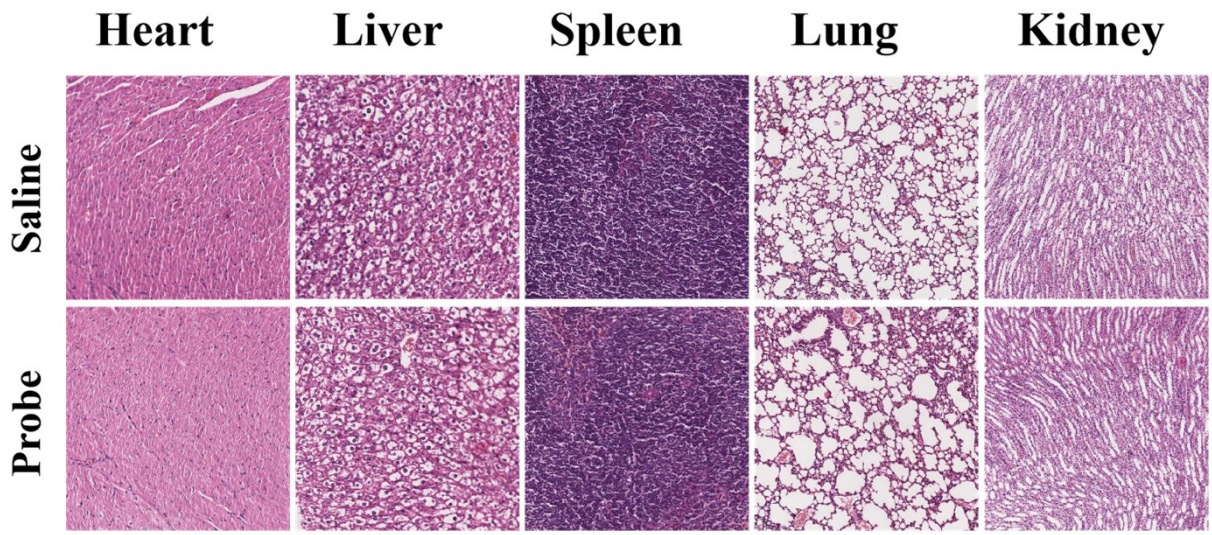

Fig. S10 Images of H&E stained main organs of the BALB/c mice intravenously injected with physiological saline and the nanoprobe [Eu(BTD)$_3$(DPBT)]-BSA@MnO_2 for 24 h.

6. TGL imaging of H_2O_2 in living cells

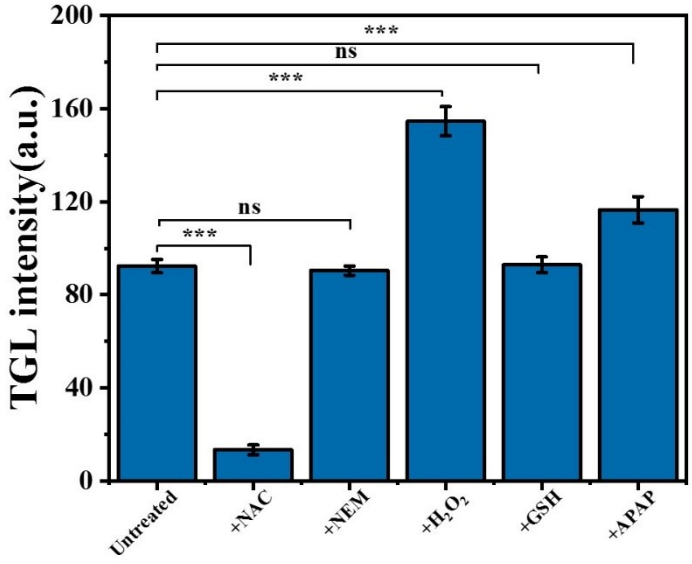

Fig. S11 Mean intracellular TGL intensities of different HeLa cells in TGL images of Figure 6. A: untreated cells, B: NAC-treated cells, C: NEM-treated cells, D: H_2O_2-treaed cells, E: GSH-treated cells, F: APAP-treated cells (*P < 0.05, **P < 0.01, ***P < 0.001).

7. TGLI of H_2O_2 in the slices of tumors from tumor-bearing BALB/c mice

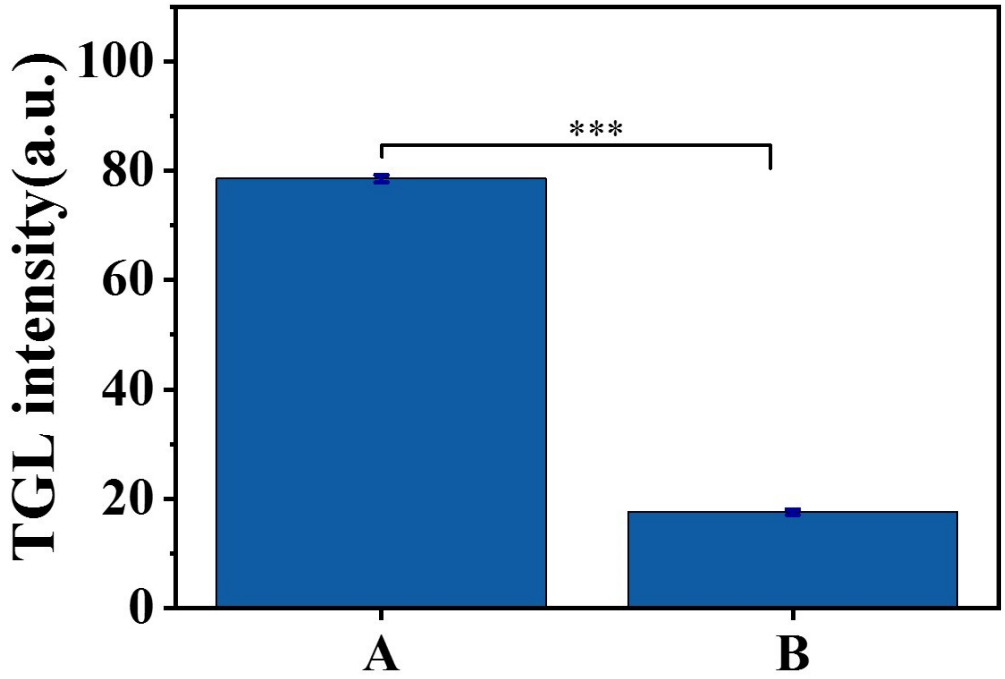

Fig. S12 Mean TGL intensities of the tissue sections in TGL images of Figure 8. (A) untreated tumor tissues; (B) NAC pretreated tumor tissues (*P < 0.05, **P < 0.01, ***P < 0.001).

Table S2 Comparison of H_2O_2 fluorescent probes

	Probe	linear detection range	detection limit	response rate	Reference
1	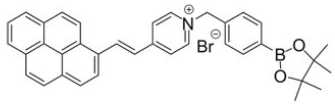 Py-VPB	0-45 μM	117 nM	45 min	5
2	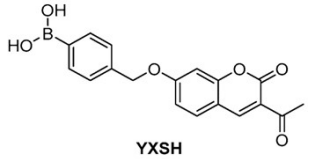 YXSH	1-100 μM	0.9 μM	5 h	6
3	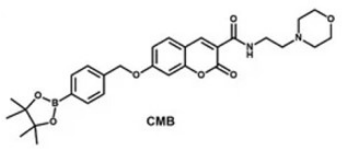 CMB	0-50 μM	0.13 μM	70 min	7
4	Ag@AuNPs-DNA/GQDs	5-200 μM	0.49 μM	2 h	8

5	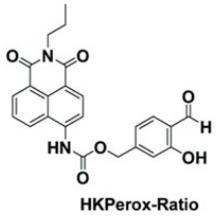 HKPerox-Ratio	0-30 μM	4.8 nM	10 min	9
6	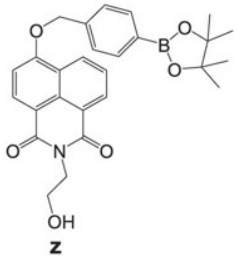 Z	2-10 μM	57 nM	15 min	10
7	ZGSCY nanoprobe	0.5–60 μM、60–400 μM	91 nM	5 min	11
8	PMT–F127 micelles	0.7–200 μM	0.95 μM	$t_{1/2}$=120 s	12
9	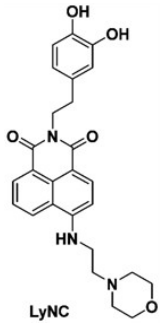 LyNC	0-220 μM	0.22 μM	60 min	13
10	Au@MnO_2@Raman reporter	60-200 μM	6.54 μM	10 min	14
11	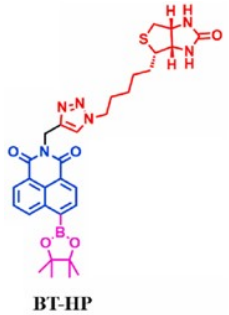 BT-HP	1-50 μM	0.15 μM	2 min	15
12	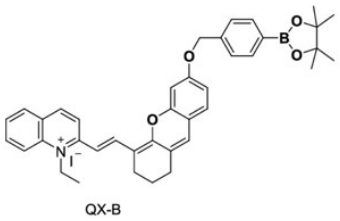 QX-B	0-50 μM	0.17 μM	5 min	16
13	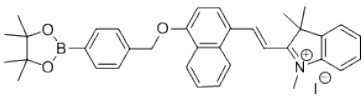 HCyHP	5-125 μM	1.74 μM	15 min	17

14	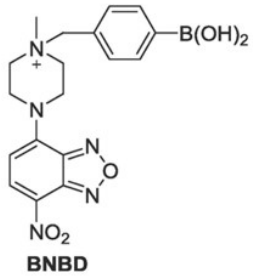 BNBD	0-14 μM	1.8 nM	20 min	18
15	[Eu(BTD)$_3$(DPBT)]-BSA@MnO_2	0-200 μM	0.87 μM	6.5 min	This work

8. References

1. Yuan Y, Wu S, Shu F, et al. An MnO_2 nanosheet as a label-free nanoplatform for homogeneous biosensing [J]. Chemical Communications, 2014, 50, 1095-1097.
2. Wu J, Wang G, Jin D, et al. Luminescent europium nanoparticles with a wide excitation range from UV to visible light for biolabeling and time-gated luminescence bioimaging [J]. Chemical Communications, 2008, 365-367.
3. Wang G, Yuan J, Matsumoto K, et al. Homogeneous Time-Resolved Fluorescence DNA Hybridization Assay by DNA-Mediated Formation of an EDTA–Eu(III)–β-Diketonate Ternary Complex [J]. Analytical Biochemistry, 2001, 299, 169-172.
4. Shen J, Sun L, Zhu J, et al, Biocompatible Bright YVO_4:Eu Nanoparticles as Versatile Optical Bioprobes [J]. Advanced Functional Materials, 2010, 20, 3707-3707.
5. Chen Q, Cheng K, Wang W, et al. A pyrene-based ratiometric fluorescent probe with a large Stokes shift for selective detection of hydrogen peroxide in living cells [J]. Journal of Pharmaceutical Analysis, 2020, 10(5): 490-7.
6. Wang K, Yao T, Xue J, et al. A Novel Fluorescent Probe for the Detection of Hydrogen Peroxide [J]. Biosensors, 2023, 13(6): 658.
7. Zuo Y, Jiao Y, Ma C, et al. A Novel Fluorescent Probe for Hydrogen Peroxide and Its Application in Bio-Imaging [J]. Molecules, 2021, 26(11): 3352.
8. Shang L-L, Song X, Niu C-B, et al. Red fluorescent nanoprobe based on Ag@Au nanoparticles and graphene quantum dots for H_2O_2 determination and living cell imaging [J]. Microchimica Acta, 2021, 188(9): 291.
9. Ye S, Hu J J, Zhao Q A, et al. Fluorescent probes for in vitro and in vivo quantification of hydrogen peroxide [J]. Chemical Science, 2020, 11(44): 11989-97.
10. Wang S, Yao J, Wang B, et al. A ratiometric and two-photon fluorescent probe for imaging hydrogen peroxide in living cells [J]. Luminescence, 2022, 37(6): 1037-43.
11. Wang L, Shi J, Wang P, et al. High-sensitive detection of H_2O_2 in biological systems by persistent luminescent nanoprobes [J]. Chemical Engineering Journal, 2024, 486: 150291.
12. Qiao J, Liu Z, Tian Y, et al. Multifunctional self-assembled polymeric nanoprobes for FRET-based ratiometric detection of mitochondrial H_2O_2 in living cells [J]. Chemical Communications, 2015, 51(17): 3641-4.
13. Reja S I, Gupta M, Gupta N, et al. A lysosome targetable fluorescent probe for endogenous imaging of hydrogen peroxide in living cells [J]. Chemical Communications, 2017, 53(26): 3701-4.
14. Zhang C, Liu X, Xu Z, et al. Multichannel Stimulus-Responsive Nanoprobes for H_2O_2 Sensing in Diverse

Biological Milieus [J]. Analytical Chemistry, 2020, 92(18): 12639-46.
15. Ren M, Dong D, Xu Q, et al. A biotin-guided two-photon fluorescent probe for detection of hydrogen peroxide in cancer cells ferroptosis process [J]. Talanta, 2021, 234: 122684.
16. Wang W-X, Jiang W-L, Mao G-J, et al. Monitoring the Fluctuation of Hydrogen Peroxide in Diabetes and Its Complications with a Novel Near-Infrared Fluorescent Probe [J]. Analytical Chemistry, 2021, 93(6): 3301-7.
17. Wang J, Zhu W, Niu G, et al. Selectively light-up hydrogen peroxide in hypoxic cancer cells with a novel fluorescent probe [J]. Chemical Communications, 2018, 54(99): 13957-60.
18. Han J, Chu C, Cao G, et al. A simple boronic acid-based fluorescent probe for selective detection of hydrogen peroxide in solutions and living cells [J]. Bioorganic Chemistry, 2018, 81: 362-6.